*Journal of Sound and Vibration* (2001) **240**(5), 837–858
doi:10.1006/jsvi.2000.3259, available online at http://www.idealibrary.com on IDEAL®

# PERIODIC MOTIONS AND GLOBAL BIFURCATIONS OF A TWO-DEGREE-OF-FREEDOM SYSTEM WITH PLASTIC VIBRO-IMPACT

G. W. Luo

*Department of Mechanical Engineering, Lanzhou Railway Institute, Lanzhou* 730070, *People's Republic of China*

J. H. Xie

*Department of Applied Mechanics and Engineering, Southwest Jiaotong University, Chengdu* 610031, *People's Republic of China*

AND

S. H. L. Guo

*Northwest Normal University, Lanzhou* 730070, *People's Republic of China*

(*Received* 15 *April* 1999, *and in final form* 26 *July* 2000)

A two-degree-of-freedom (d.o.f.) impact system with proportional damping is considered. The maximum displacement of one of the masses is limited to a threshold value by a rigid wall, which gives rise to a non-linearity in the system. A limiting case of a dynamical problem arising in the mechanical systems with amplitude constraints is investigated. For the perfectly plastic vibro-impact case, dynamics of a two-degree-of-freedom vibratory system contacting a single stop is represented by a three-dimensional map. Existence and stability of period $n$ single-impact motions are analyzed by analytical and numerical methods. It is shown that the vibro-impact system may exhibit two different types of periodic motions due to the piecewise property of the map. Transitions of two types of period $n$ single-impact motions are demonstrated. The singularities of the Poincaré map, caused by grazing boundary motion of the impact oscillator, are considered. Due to the piecewise discontinuities and singularities of the map, the vibro-impact system is shown to undergo period-doubling bifurcations followed by complex sequence of transitions, in which the period-doubling cascades do not occur and extremely long-periodic and chaotic motions are generated directly with the motions with grazing boundary occurring. Finally, the influence of system parameters on periodic impacts and global bifurcations is discussed.



## 1. INTRODUCTION

Vibrating systems with clearances between the moving parts are frequently encountered in a large number of diverse engineering fields. Impacts occur when the amplitudes of vibration of some parts of the systems exceed critical values. Research for vibro-impact problems has important significance on optimization design of machinery with clearances or gaps, reliability analyses and noise suppression, etc. Because the physical process during impacts is strongly non-linear and discontinuous, the vibro-impact systems can exhibit very rich and complicated dynamic behaviour. In recent years, many new problems of theory have been advanced in research of vibro-impact problems so that it becomes a new subject

0022-460X/01/100837 + 22 $35.00/0 

on non-linear dynamics. Some researches, including singularity [1–8], "*inelastic*" vibroimpacts [9–12], high-codimension bifurcation [13] and quasi-periodic impacts [14–18], were unfolded for the vibro-impact systems. Dynamics and bifurcations of one-degree-of-freedom plastic vibro-impact systems were studied in references [9–11]. For the inelastic vibro-impact case, Shaw and Holmes [9, 10] studied the motions of a oscillator with harmonic excitation and a constraint by using a one-dimensional map, which is represented by piecewise maps on circle. Analysis of this map shows that stable periodic orbits exist at almost all forcing frequencies but that transient non-periodic or chaotic motions can also occur. Xie [11] represented the dynamics of one-degree-of-freedom impact hammer by a one-dimensional map on circle and described the properties of the map. It is found that the bifurcational behaviours of the impact hammer were different from that of usual one-dimensional consecutive maps [19]. But the interruption of period-doubling cascades and the transition to chaos were not analyzed for the one-degree-of-freedom impact hammer in reference [11].

The plastic vibro-impact systems considered in references [9–11] are all single-degree-of-freedom ones. But the vibro-impact systems in engineering fields are usually multi-degree-of-freedom ones. In the paper, we consider a two-degree-of-freedom system with harmonic excitations and a constraint. Peterka [12] and Aidanpää [20] have studied dynamics and bifurcations of the mechanical model for elastic vibro-impact case. The purpose of the present study is to focus attention on the periodic motions and global bifurcations of such system in the perfectly plastic vibro-impact case. On the perfectly plastic impact condition, dynamics of the system is represented by a three-dimensional map, which is of piecewise property and singularities caused by the motion with grazing boundary. The influence of singularities on global bifurcations and the transitions to chaos is elucidated. It is found that the vibro-impact system goes through complicated dynamic evolution beyond period-doubling bifurcations with increase in the excitation frequency. Period-doubling bifurcations of periodic motions with one impact are commonly existent, but the period-doubling cascades are non-existent under a smooth change in the excitation frequency. After period-doubling bifurcations of periodic motions with single-impact occur, the system may exhibit the motions with grazing boundary so that extremely long periodic and chaotic motions are generated immediately. The phenomena of grazing boundary were analyzed in the research of dynamics of elastic vibro-impact systems [1, 5]. The influences of system parameters such as distribution of mass and stiffness, damping ratio and clearance on periodic impacts and global bifurcations are discussed briefly.

## 2. PERIODIC MOTIONS WITH SINGLE IMPACT

The mechanical model for a two-degree-of-freedom vibrator with masses $M_1$ and $M_2$ is shown in Figure 1. The masses are connected to linear springs with stiffnesses $K_1$ and $K_2$. The excitations on both masses are harmonic with amplitudes $P_1$ and $P_2$. The excitation

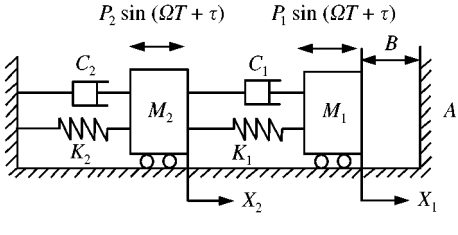


Figure 1. Schematic of the two-degree-of-freedom impact oscillator.

frequency $\Omega$ and the phase $\tau$ are the same for both masses. The mass $M_1$ impacts against a rigid surface $A$ when its displacement $X_1(t)$ equals the gap $B$. The impact is described by a coefficient of restitution $R$. Here a special case of perfectly plastic impact is considered, in which the coefficient of restitution $R$ equals zero. When the mass $M_1$ impacts against the stop $A$, kinetic energy of the mass $M_1$ is dissipated on impact and the mass $M_1$ essentially sticks to the stop. There is no elastic rebound. However, the forces, which act on the mass $M_1$, may drive it off the stop again. Then the system begins to motion in new initial conditions and the mass $M_1$ will strike the stop again, thus and so reciprocating motions. Damping in the mechanical model is assumed as proportional damping of the Rayleigh type, which in this case implies $K_1/K_2 = C_1/C_2$.

The motion processes of the system, between any two consecutive impacts, are considered. Between any two consecutive impacts, the time $T$ is set to zero directly at the instant when the former impact finishes, and the phase angle $\tau$ is used only to make a suitable choice for the origin of time in the calculation. The state of the vibro-impact system, immediately after impact, becomes initial conditions of the system in the subsequent process of motion. Let $X_{20}$ and $\dot{X}_{20}$ represent, respectively, displacement and velocity of the mass $M_2$ at the instant of the former impact. The velocity of the mass $M_1$ varies from $\dot{X}_{1-}$ and $\dot{X}_{1+} = 0$ at the moment when it impacts the stop. When $\dot{X}_{1-}$ and $\dot{X}_{1+}$ represent the impacting mass velocities of approach and departure at the instant of impact respectively. Let $F_1$ represent a resultant force, which consists of spring restoring force, damping force and sinusoidal excitation acted on the mass $M_1$, i.e.,

$$F_1 = K_1(X_2 - X_1) + C_1(\dot{X}_2 - \dot{X}_1) + P_1 \sin(\Omega T + \tau). \tag{1}$$

If the resultant force $F_1$, at the instant when the former impact is over, is in the positive direction, i.e.,

$$F_1 = K_1(X_{20} - B) + C_1\dot{X}_{20} + P_1 \sin\tau > 0, \tag{2}$$

the force simply push the mass $M_1$ against the stop, with which it remains in contact. The two-degree-of-freedom vibro-impact system becomes a single-degree-of-freedom oscillator subjected to sinusoidal excitation, and its differential equation of motion is

$$M_2\dot{X}_2 + (C_1 + C_2)\dot{X}_2 + (K_1 + K_2)X_2 - K_1B = P_2 \sin(\Omega T + \tau). \tag{3}$$

Until the resultant force $F_1$ changes its direction (sign), the force begins to push the mass $M_1$ away from the stop again, and the single-degree-of-freedom oscillator becomes a two-degree-of-freedom vibro-impact system. Let $T_s$ represent the time during which the mass $M_1$ is in contact with the stop. If there exists $\varepsilon_1 > 0$, and

$$K_1(\bar{X}_{20} - B) + C_1\dot{\bar{X}}_{20} + P_1 \sin(\Omega T + \tau) = 0, \quad T = T_s, \tag{4}$$

$$K_1(X_2 - X_1) + C_1(\dot{X}_2 - \dot{X}_1) + P_1 \sin(\Omega T + \tau) < 0, \quad T_s < T < T_s + \varepsilon_1, \tag{5}$$

then the forcing $F_1$ will drive the mass $M_1$ off the stop. Here $\bar{X}_{20}$ and $\dot{\bar{X}}_{20}$ represent, respectively, displacement and velocity of the mass $M_2$ at the time $T = T_s$.

If the resultant force $F_1$ acted on the mass $M_1$ which is in the negative direction immediately after impact, i.e.,

$$K_1(X_{20} - B) + C_1\dot{X}_{20} + P_1 \sin\tau < 0, \tag{6}$$

then the force $F_1$ immediately drives the mass $M_1$ off the stop. The mass $M_1$ spends no time stuck to the stop, and moves in the opposite direction with initial velocity $\dot{X}_1 = 0$.

A special case must be considered, in which the resultant force $F_1$ equals zero when the mass $M_1$ impacts the stop. If $F_1$ changes in positive direction immediately at the instant when the impact is over, then the mass $M_1$ will stick to the stop; otherwise the force $F_1$ will drive it off the stop immediately.

Between two consecutive impacts, the differential equations of motion, written in the non-dimensional form, are given by

$$\dot{x}_1 = \dot{x}_{1-} \quad (x_1 = b,\, t = 0_-), \qquad \dot{x}_1 = \dot{x}_{1+} = 0 \quad (x_1 = b, \quad 0_+ \leqslant t \leqslant t_s), \tag{7}$$

$$\mu_m \ddot{x}_2 + 2\zeta(1+\mu_c)\dot{x}_2 + (1+\mu_k)x_2 - b = \bar{f}_{20}\sin(\omega t + \tau) \quad (0_+ \leqslant t \leqslant t_s), \tag{8}$$

$$\begin{bmatrix} 1 & 0 \\ 0 & \mu_m \end{bmatrix} \begin{Bmatrix} \ddot{x}_1 \\ \ddot{x}_2 \end{Bmatrix} + \begin{bmatrix} 2\zeta & -2\zeta \\ -2\zeta & 2\zeta(1+\mu_c) \end{bmatrix} \begin{Bmatrix} \dot{x}_1 \\ \dot{x}_2 \end{Bmatrix} + \begin{bmatrix} 1 & -1 \\ -1 & 1+\mu_k \end{bmatrix} \begin{Bmatrix} x_1 \\ x_2 \end{Bmatrix}$$
$$= \begin{Bmatrix} \bar{f}_{10} \\ \bar{f}_{20} \end{Bmatrix} \sin(\omega t + \tau + \omega t_s) \quad (t_s \leqslant t \leqslant t_s + t_f). \tag{9}$$

In Equations (7)–(9), a dot " $\cdot$ " denotes differentiation with respect to the non-dimensional time $t$, $t_f$ denotes the flight time of the mass $M_1$, between two successive impacts, $t_s$ is the non-dimensional expression of the time $T_s$. $t_s + t_f$ denotes the time interval between two successive impacts, where the non-dimensional quantities

$$\mu_m = \frac{M_2}{M_1}, \quad \mu_k = \frac{K_2}{K_1}, \quad \mu_c = \mu_k, \quad \bar{f}_{20} = \frac{P_2}{P_1 + P_2}, \quad \bar{f}_{10} = 1 - \bar{f}_{20}, \quad \omega = \Omega\sqrt{\frac{M_1}{K_1}}, \tag{10}$$

$$t = T\sqrt{\frac{K_1}{M_1}}, \quad \zeta = \frac{C_1}{2\sqrt{K_1 M_1}}, \quad b = \frac{BK_1}{P_1 + P_2}, \quad x_1 = \frac{X_i K_1}{P_1 + P_2}, \quad \dot{x}_i = \frac{\dot{X}_i\sqrt{M_1 K_1}}{P_1 + P_2}, \quad i = 1, 2$$

have been introduced.

Formulae (2)–(6) are rewritten in non-dimensional form

$$(x_{20} - b) + 2\zeta\dot{x}_{20} + \bar{f}_{10}\sin\tau > 0, \tag{11}$$

$$\begin{aligned} &(\bar{x}_{20} - b) + 2\zeta\dot{\bar{x}}_{20} + \bar{f}_{10}\sin(\omega t + \tau) = 0, \qquad t = t_s, \\ &(x_2 - x_1) + 2\zeta(\dot{x}_2 - \dot{x}_1) + \bar{f}_{10}\sin(\omega t + \tau) < 0, \quad t_s < t < t_s + \varepsilon_1', \end{aligned} \tag{12}$$

$$(x_{20} - b) + 2\zeta\ddot{x}_{20} + \bar{f}_{10}\sin\tau < 0, \tag{13}$$

where $\bar{x}_{20}$ and $\dot{\bar{x}}_{20}$ represent, respectively, non-dimensional displacement and velocity of the mass $M_2$ at the time $t = t_s$.

For $0_+ \leqslant t \leqslant t_s$, The two-degree-of-freedom system contacting a single stop becomes a single-degree-of-freedom oscillator subjected to sinusoidal excitation, and the general solutions of equation (8) are given by

$$\begin{aligned} x_1(t) &= b, \qquad \dot{x}_1(t) = 0, \\ x_2(t) &= \mathrm{e}^{-\zeta\omega_0^2 t}(c\cos\omega_d t + d\sin\omega_d t) + A_0\sin(\omega t + \tau) + B_0\cos(\omega t + \tau) + x_0, \\ \dot{x}_2(t) &= \mathrm{e}^{-\zeta\omega_0^2 t}((d\omega_d - c\zeta\omega_0^2)\cos\omega_d t - (d\zeta\omega_0^2 + c\omega_d)\sin\omega_d t) + A_0\omega\cos(\omega t + \tau) \\ &\quad - B_0\omega\sin(\omega t + \tau), \end{aligned} \tag{14}$$

where $\omega_0^2 = (1 + \mu_k)/\mu_m$, $\omega_d = \omega_0\sqrt{1 - \zeta^2\omega_0^2}$, $x_0 = b/(1 + \mu_k)$, and

$$c = x_{20} - x_0 - A_0 \sin\tau - B_0 \cos\tau, \tag{15}$$

$$d = \frac{\dot{x}_{20} + \zeta\omega_0^2(x_{20} - x_0) - (A_0\zeta\omega_0^2 - B_0\omega)\sin\tau - (B_0\zeta\omega_0^2 + A_0\omega)\cos\tau}{\omega_d}, \tag{16}$$

$$A_0 = \frac{(\omega_0^2 - \omega^2)\bar{f}_0}{(\omega_0^2 - \omega^2)^2 + (2\zeta\omega\omega_0^2)^2}, \qquad B_0 = \frac{2\zeta\omega\omega_0^2\bar{f}_0}{(\omega_0^2 - \omega^2)^2 + (2\zeta\omega\omega_0^2)^2}, \tag{17}$$

where $\bar{f}_0 = \bar{f}_{20}/\mu_m$.

Let $\psi$ represent the canonical model matrix of equations (9). $\omega_1$ and $\omega_2$ denote the eigenfrequencies of the system as impacts do not occur. Taking $\psi$ as a transition matrix, equations of motion (9), under the change of variables

$$X = \psi\xi, \tag{18}$$

becomes

$$I\ddot{\xi} + C\dot{\xi} + \Lambda\xi = \bar{F}\sin(\omega t + \tau), \tag{19}$$

where $X = (x_1, x_2)^{\mathrm{T}}$, $\xi = (\xi_1, \xi_2)^{\mathrm{T}}$, $I$ is an unit matrix of degree $2 \times 2$, $C$ and $\Lambda$ are diagonal matrices, and $C = \mathrm{diag}[2\xi\omega_1^2, 2\zeta\omega_2^2]$, $\Lambda = \mathrm{diag}[\omega_1^2, \omega_2^2]$, $F = (\bar{f}_1, \bar{f}_2)^{\mathrm{T}} = \psi^{\mathrm{T}}P$, $P = (1 - \bar{f}_{20}, \bar{f}_{20})^{\mathrm{T}}$. $\xi$ is the response of the system for $t \in [t_s, t_s + t_f]$, in the canonical co-ordinates. Equations of motion (9) are resolved by using formal co-ordinate and modal matrix approach. The general solutions of equations (9) take the form

$$x_i(t) = \sum_{j=1}^{2} \psi_{ij}(\mathrm{e}^{-\eta_j(t-t_s)}(a_j \cos\omega_{dj}(t - t_s) + b_j \sin\omega_{dj}(t - t_s)) + A_j \sin(\omega(t - t_s) + \tau + \beta) + B_j \cos(\omega(t - t_s) + \tau + \beta)), \tag{20}$$

$$\dot{x}_i(t) = \sum_{j=1}^{2} \psi_{ij}(\mathrm{e}^{-\eta_j(t-t_s)}((b_j\omega_{dj} - \eta_j a_j)\cos\omega_{dj}(t - t_s) - (a_j\omega_{dj} + \eta_j b_j)\sin\omega_{dj}(t - t_s)) + A_1\omega\cos(\omega(t - t_s) + \tau + \beta) - B_j\omega\sin(\omega(t - t_s) + \tau + \beta)) \quad (i = 1, 2), \tag{21}$$

where $t_s \leqslant t \leqslant t_s + t_f$, $\beta = \omega t_s$, $t_f$ denotes the flight time of the mass $M_1$ between two successive impacts. $\psi_{ij}$ are the elements of the canonical modal matrix $\psi$, $\eta_j = \zeta\omega_j^2$, $\omega_{dj} = \sqrt{\omega_j^2 - \eta_j^2}$, $a_j$ and $b_j$ are the constants of integration which are determined by the initial condition and modal parameters of the system. $A_j$ and $B_j$ are the amplitude parameter, which are given by

$$A_j = \frac{1}{2\omega_{dj}}\left(\frac{\omega + \omega_{dj}}{(\omega + \omega_{dj})^2 + \eta_j^2} - \frac{\omega - \omega_{dj}}{(\omega + \omega_{dj})^2 + \eta_j^2}\right)\bar{f}_j, \tag{22}$$

$$B_j = \frac{\eta_j}{2\omega_{dj}}\left(\frac{1}{(\omega - \omega_{dj})^2 + \eta_j^2} - \frac{1}{(\omega + \omega_{dj})^2 + \eta_j^2}\right)\bar{f}_j. \tag{23}$$

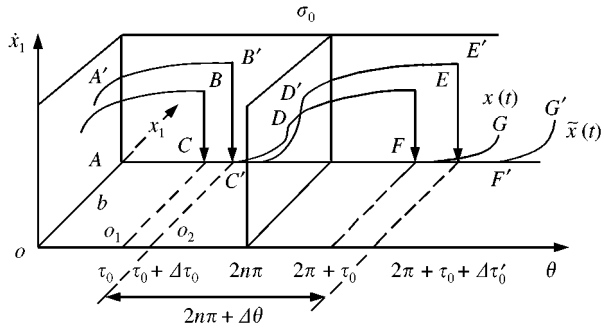


Figure 2. An extended phase space figure of the mass $M_1$.

In the extended phase space (Figure 2), the non-smooth curves $x_1(t)$ ($ABCDE$) and $\tilde{x}_1(t)(A'B'C'D'E')$ indicate, respectively, the period $n$ single-impact orbit of the mass $M_1$ and its disturbed motion. The governing points on the phase orbits show the boundary and continuity conditions of the vibro-impact system. There are generally two ways to choose a Poincaré section: $\bar{\sigma}$, $\sigma \subset \mathbf{R}^4 \times \mathbf{S}$,

$$\bar{\sigma} = \{(x_1, \dot{x}_1, x_2, \dot{x}_2, \theta) \in \mathbf{R}^4 \times \mathbf{S}, \theta = 0 \bmod(2\pi)\}, \tag{24}$$

$$\sigma = \{(x_1, \dot{x}_1, x_2, \dot{x}_2, \theta) \in \mathbf{R}^4 \times \mathbf{S}, \quad x_1 = b, \dot{x}_1 = \dot{x}_{1+} = 0\}. \tag{25}$$

Because there exists singularity of the Poincaré map caused by the motions with grazing boundary in vibro-impact systems [1, 2], it is difficult to observe the motions with grazing boundary in the Poincaré section $\bar{\sigma}$. In this paper, we choose the section $\sigma$ to establish the Poincaré map. By virtue of equations (7)–(9), the Poincaré map can be established as

$$\Delta X' = f(v, \Delta X), \tag{26}$$

where $v$ is a real parameter, $v \in \mathbf{R}^1$, $\Delta X = (\Delta x_2, \Delta \dot{x}_2, \Delta\tau)^{\mathrm{T}}$, $\Delta X' = (\Delta x_2', \Delta \dot{x}_2', \Delta\tau')^{\mathrm{T}}$ are the disturbed vectors in the hyperplane $\sigma$.

Under suitable system parameter conditions, the system given in Figure 1 can exhibit periodic behaviour. The periodic behaviour means that if the dimensionless time $t$ is set to zero directly after an impact, it becomes $2n\pi/\omega$ just before the next impact. Here $n$ stands for the number of forcing cycles between two consecutive impacts. After the origin of $\theta$-co-ordinate is displaced to an impact point $o_1$, the determination of the period $n$ single-impact motions is based on the fact that they satisfy the following set of periodicity and matching conditions:

$$x_1(t) = b(0 \leqslant t \leqslant t_s), \qquad x_1(t_s + t_f) = b, \qquad \dot{x}_1(t) = 0(0 \leqslant t \leqslant t_s), \qquad \dot{x}_{1+}(t_s + t_f) = 0,$$

$$x_2(t_s) = \bar{x}_{20}, \qquad x_2(0) = x_2(t_s + t_f) = x_{20}, \qquad \dot{x}_2(t_s) = \dot{\bar{x}}_{20}, \qquad \dot{x}_2(0) = \dot{x}_2(t_s + t_f) = \dot{x}_{20},$$

$$\omega(t_s + t_f) = 2\pi n, \qquad t = 0 \bmod 2n\pi/\omega, \qquad \tau = \tau_0 (\bmod 2n\pi/\omega), \tag{27}$$

where $X^* = (\dot{x}_{20}, x_{20}, \tau_0)^{\mathrm{T}}$ denotes a fixed point of period $n$ single-impact orbit in Poincaré section $\sigma$. We represent periodic motions of the system contacting a single stop by symbol $n$–$p$, $n$ and $p$ representing, respectively, the number of the forcing cycle and the number of impacts.

Period $n$ single-impact solution of the vibro-impact system may be written in the form

$$x_1(t) = b \quad (0 \leqslant t \leqslant t_s),$$

$$x_2(t) = e^{-\zeta\omega_0^2 t}(c\cos\omega_d t + d\sin\omega_d t) + A_0\sin(\omega t + \tau_0) + B_0\cos(\omega t + \tau_0) \quad (0 \leqslant t \leqslant t_s),$$

$$x_i(t) = \sum_{j=1}^{2} \psi_{ij}(e^{-\eta_j(t-t_s)}(a_j\cos\omega_{dj}(t-t_s) + b_j\sin\omega_{dj}(t-t_s)) + A_j\sin(\omega(t-t_s) + \tau_0 + \beta)$$
$$+ B_j\cos(\omega(t-t_s) + \tau_0 + \beta)) \quad (t_s \leqslant t \leqslant 2n\pi/\omega) \quad (i = 1, 2), \tag{28}$$

which correspond to one impact during $n$ cycle of the forcing, i.e. $t = 0 \bmod(2n\pi/\omega)$. In the period $n$ single-impact motions, the mass $M_1$ impacts the stop once during $n$ cycle of the forcing. When the mass $M_1$ impacts the stop, it is pushed away from the stop by the resultant force $F_1$ immediately, or it is pushed against the stop by the force $F_1$ until the force changes its sign. The former case, in which $M_1$ is pushed away from the stop by the force immediately, is represented by the symbol (I); the latter is represented by (II). Two definitions are required: $n - \mathrm{I} - (\mathrm{I})$ represents a type of motion, in which there exists one impact during $n$ cycle of the forcing and $M_1$ does not stick to the stop; $n - 1 - (\mathrm{II})$ represents another type of motion, in which there exists one impact during $n$ cycle of the forcing and the mass $M_1$ remains in contact with the stop until the resultant force $F_1$ change its sign.

## 3. POINCARE MAPS OF PERIOD $N$ SINGLE-IMPACT ORBITS

We first consider the perturbed motion of $n - 1 - (\mathrm{II})$ periodic orbit to determine the equation of map. For simplicity of notation, the origin of time is chosen at the impact point. The origin of $\theta$-co-ordinate is displaced to an impact point $o_2$ in Figure 2. Here $\tilde{X} = (\tilde{x}_1, \bar{x}_2)^{\mathrm{T}}$ and $\dot{\tilde{X}} = (\dot{\tilde{x}}_1, \dot{\tilde{x}}_2)^{\mathrm{T}}$ represent displacements and velocities in the perturbed motion respectively. Between two consecutive impacts, for $\tilde{x}_1 \leqslant b$, the solutions of the perturbed motion are given by

$$\tilde{x}_1(t) = b \quad (0 \leqslant t \leqslant \tilde{t}_s),$$

$$\tilde{x}_2(t) = e^{-\zeta\omega_0^2 t}(\tilde{c}\cos\omega_d t + \tilde{d}\sin\omega_d t) + A_0\sin(\omega t + \tau_0 + \Delta\tau) + B_0\cos(\omega t + \tau_0 + \Delta\tau)$$
$$(0 \leqslant t \leqslant \tilde{t}_s),$$

$$\tilde{x}_i(t) = \sum_{j=1}^{2} \psi_{ij}\tilde{\xi}_j(t) \qquad (\tilde{t}_s \leqslant t \leqslant (2n\pi + \Delta\theta)/\omega) \quad (i = 1, 2), \tag{29}$$

where

$$\tilde{\xi}_j(t) = e^{-\eta_j(t-\tilde{t}_s)}(\tilde{a}_j\cos\omega_{dj}(t-\tilde{t}_s) + \tilde{b}_j\sin\omega_{dj}(t-\tilde{t}_s)) + A_j\sin(\omega(t-\tilde{t}_s) + \tau_0 + \Delta\tau + \beta + \Delta\beta) \tag{30}$$
$$+ B_j\cos(\omega(t-\tilde{t}_s) + \tau_0 + \Delta\tau + \beta + \Delta\beta),$$

in which, $\beta = \omega t_s$, $\Delta\beta = \omega\Delta t_s$, $\tilde{t}_s = t_s + \Delta t_s$.

For the disturbed motion shown in Figure 2, the dimensionless time $t$ is set to zero directly immediately after impact, it becomes $(2n\pi + \Delta\theta)/\omega$ just before the next impact, and $\Delta\theta = \Delta\tau' - \Delta\tau$. Letting $t_e = (2n\pi + \Delta\theta)/\omega$, the boundary conditions at two successive impact points are given by

$$\begin{aligned}
&\tilde{x}_1(t) = b(0 \leqslant t \leqslant \tilde{t}_s), \qquad \tilde{x}_1(t_e) = b, \qquad \dot{\tilde{x}}_1(t) = 0(0 \leqslant t \leqslant \tilde{t}_s),\\
&\tilde{x}_2(\tilde{t}_s) = \bar{x}_{20} + \Delta\bar{x}_{20}, \qquad \tilde{x}_2(0) = x_{20} + \Delta x_{20}, \qquad \tilde{x}_2(t_e) = x_{20} + \Delta x'_{20},\\
&\dot{\tilde{x}}_2(\tilde{t}_s) = \dot{\bar{x}}_{20} + \Delta\dot{\bar{x}}_{20}, \qquad \dot{\tilde{x}}_2(0) = \dot{x}_{20} + \Delta\dot{x}_{20}, \qquad \dot{\tilde{x}}_2(t_e) = \dot{x}_{20} + \Delta\dot{x}'_{20},
\end{aligned} \tag{31}$$

in which, $\tilde{t}_s = t_s + \Delta t_s$, $\Delta X = (\Delta x_{20}, \Delta\dot{x}_{20}, \Delta\tau)^{\mathrm{T}}$ and $\Delta X' = (\Delta x'_{20}, \Delta\dot{x}'_{20}, \Delta\tau')^{\mathrm{T}}$ are the disturbed vectors of fixed point $X^* = (x_{20}, \dot{x}_{20}, \tau)^{\mathrm{T}}$, and

$$t_e = t_s + \Delta t_s + t_f + \Delta t_f, \qquad 2\pi n + \Delta\theta = \omega(t_s + \Delta t_s + t_f + \Delta t_f). \tag{32}$$

Inserting boundary conditions (31) into solutions (29) of the perturbed motion for $t = 0$, we can solve for

$$\tilde{c} = x_{20} + \Delta x_{20} - x_0 - A_0 \sin(\tau_0 + \Delta\tau) - B_0 \cos(\tau_0 + \Delta\tau), \tag{33}$$

$$\tilde{d} = \frac{d_1 - (A_0\zeta\omega_0^2 - B_0\omega)\sin(\tau_0 + \Delta\tau) - (B_0\zeta\omega_0^2 + A_0\omega)\cos(\tau_0 + \Delta\tau)}{\omega_d}, \tag{34}$$

where $d_1 = \dot{x}_{20} + \Delta\dot{x}_{20} + \zeta\omega_0^2(x_{20} + \Delta x_{20} - x_0)$.

Inserting boundary conditions (31) into the solutions of the perturbed motion for $t = \tilde{t}_s$, we can solve for

$$\begin{aligned}
\bar{x}_{20} + \Delta\bar{x}_{20} = {} & \mathrm{e}^{-\zeta\omega_0^2(t_s + \Delta t_s)}(\tilde{c}\cos\omega_d(t_s + \Delta t_s) + \tilde{d}\sinh\omega_d(t_s + \Delta t_s))\\
& + A_0\sin(\omega(t_s + \Delta t_s) + \tau_0 + \Delta\tau) + B_0\cos(\omega(t_s + \Delta t_s) + \tau_0 + \Delta\tau) + x_0,
\end{aligned} \tag{35}$$

$$\begin{aligned}
\dot{\bar{x}}_{20} + \Delta\dot{\bar{x}}_{20} = {} & \mathrm{e}^{-\zeta\omega_0^2(t_s + \Delta t_s)}((\tilde{d}\omega_d - \tilde{c}\zeta\omega_0^2)\cos\omega_d(t_s + \Delta t_s) - (\tilde{d}\zeta\omega_0^2 + \tilde{c}\omega_d)\sin\omega_d(t_s + \Delta t_s))\\
& + A_0\omega\cos(\omega(t_s + \Delta t_s) + \tau_0 + \Delta\tau) - B_0\omega\sin(\omega(t_s + \Delta t_s) + \tau + \Delta\tau),
\end{aligned} \tag{36}$$

$$\tilde{a}_1 = \frac{1}{D}(\psi_{22}b - \psi_{12}(\bar{x}_{20} + \Delta\bar{x}_{20}) - DA_1\sin(\tau_0 + \Delta\tau + \beta + \Delta\beta) - DB_1\cos(\tau_0 + \Delta\tau + \beta + \Delta\beta)), \tag{37}$$

$$\tilde{a}_2 = \frac{1}{D}(\psi_{11}(\bar{x}_{20} + \Delta\bar{x}_{20}) - \psi_{21}b - DA_2\sin(\tau_0 + \Delta\tau + \beta + \Delta\beta) - DB_2\cos(\tau_0 + \Delta\tau + \beta + \Delta\beta), \tag{38}$$

$$\begin{aligned}
\tilde{b}_1 = {} & \frac{1}{D\omega_1}(\psi_{22}\eta_1 b - \psi_{12}(\dot{\bar{x}}_{20} + \Delta\dot{\bar{x}}_{20} + \eta_1\bar{x}_{20} + \eta_1\Delta\bar{x}_{20}) - D(A_1\omega + \eta_1 B_1)\\
& \times\cos(\tau_0 + \Delta\tau + \beta + \Delta\beta) + D(B_1\omega - \eta_1 A_1)\sin(\tau_0 + \Delta\tau + \beta + \Delta\beta)),
\end{aligned} \tag{39}$$

$$\begin{aligned}
\tilde{b}_2 = {} & \frac{1}{D\omega_2}(-\psi_{21}\eta_2 b + \psi_{11}(\dot{\bar{x}}_{20} + \Delta\dot{\bar{x}}_{20} + \eta_2(\bar{x}_{20} + \Delta\bar{x}_{20})) - D(A_2\omega + \eta_2 B_2)\\
& \times\cos(\tau_0 + \Delta\tau + \beta + \Delta\beta) + D(B_2\omega - \eta_2 A_2)\sin(\tau_0 + \Delta\tau + \beta + \Delta\beta)),
\end{aligned} \tag{40}$$

where $D = |\psi|$.

Applying boundary conditions (31) to equations (12) for $t = \tilde{t}_s$, we can obtain

$$\bar{x}_{20} + \Delta\bar{x}_{20} - b + 2\zeta(\dot{\bar{x}}_{20} + \Delta\dot{\bar{x}}_{20}) + \bar{f}_{10}\sin(\omega(t_s + \Delta t_s) + \tau_0 + \Delta\tau) = 0. \tag{41}$$

Defining a function $h(\Delta x_{20}, \Delta\dot{x}_{20}, \Delta\tau, \Delta t_s)$ as

$$\begin{aligned} h(\Delta x_{20}, \Delta\dot{x}_{20}, \Delta\tau, \Delta t_s) = {} & \bar{x}_{20} + \Delta\bar{x}_{20} - b + 2\zeta(\dot{\bar{x}}_{20} + \Delta\dot{\bar{x}}_{20}) \\ & + \bar{f}_{10}\sin(\omega(t_s + \Delta t_s) + \tau_0 + \Delta\tau) = 0. \end{aligned} \tag{42}$$

Suppose $\partial h/\partial\Delta t_s|_{(0,0,0,0)} \neq 0$, according to the implicit function theorem, equation (42) can be solved for

$$\Delta t_s = \Delta t_s(\Delta x_{20}, \Delta\dot{x}_{20}, \Delta\tau), \qquad \Delta t_s(0, 0, 0) = 0. \tag{43}$$

Let $\Delta X = (y_1, y_2, y_3)^{\mathrm{T}} = (\Delta x_{20}, \Delta\dot{x}_{20}, \Delta\tau)^{\mathrm{T}}$, it is easy to obtain the following derivatives:

$$\frac{\partial\Delta t_s}{\partial y_j} = -\frac{\partial h}{\partial y_j}\Big/\frac{\partial h}{\partial\Delta t_s}, \quad j = 1, 2, 3. \tag{44}$$

Using solutions (29) of the perturbed motion, we can obtain

$$b = \sum_{j=1}^{2} \psi_{1j}\tilde{\xi}_j(t_e). \tag{45}$$

Define a function $g(\Delta x_{20}, \Delta\dot{x}_{20}, \Delta\tau, \Delta t_s, \Delta t_f)$ as

$$g(\Delta x_{20}, \Delta\dot{x}_{20}, \Delta\tau, \Delta t_s, \Delta t_f) = \sum_{j=1}^{2} \psi_{1j}\tilde{\xi}_j(t_e) - b = 0. \tag{46}$$

Suppose $\partial g/\partial\Delta t_f|_{(0,0,0,0)} \neq 0$, according to the implicit function theorem, equation (46) can be solved for

$$\Delta t_f = \Delta t_f(\Delta x_{20}, \Delta\dot{x}_{20}, \Delta\tau, \Delta t_s), \qquad \Delta t_f(0, 0, 0, 0) = 0. \tag{47}$$

Using equations (43) and (47), we have

$$\frac{\partial\Delta t_f}{\partial y_j} = -\left(\frac{\partial g}{\partial y_j} + \frac{\partial g}{\partial\Delta t_s}\cdot\frac{\partial\Delta t_s}{\partial y_j}\right)\Big/\frac{\partial g}{\partial\Delta t_f} \quad (j = 1, 2, 3). \tag{48}$$

Inserting formulae (37)–(40) and boundary conditions (31) to solutions (29) of the perturbed motion, we get finally the Poincaré map, corresponding to $n - 1 -$ (II) orbit, which is given by

$$\Delta x'_{20} = \sum_{j=1}^{2} \psi_{2j}\tilde{\xi}_j(t_e) - x_{20}, \qquad \Delta\dot{x}'_{20} = \sum_{j=1}^{2} \psi_{2j}\dot{\tilde{\xi}}_j(t_e) - \dot{x}_{20}, \qquad \Delta\tau' = \Delta\tau + \omega\Delta t_s + \omega\Delta t_f, \tag{49}$$

where

$$\begin{aligned} \dot{\tilde{\xi}}_j(t) = {} & \mathrm{e}^{-\eta_j(t-\tilde{t}_s)}((\tilde{b}_j\omega_{dj} - \eta_j\tilde{a}_j)\cos\omega_{dj}(t - \tilde{t}_s) - (\eta_j\tilde{b}_j + \tilde{a}_j\omega_{dj})\sin\omega_{dj}(t - \tilde{t}_s)) \\ & + A_j\omega\cos(\omega(t - \tilde{t}_s) + \tau_0 + \Delta\tau + \beta + \Delta\beta) - B_j\omega\sin(\omega(t - \tilde{t}_s) + \tau_0 + \Delta\tau + \beta + \Delta\beta). \end{aligned} \tag{50}$$

Introducing solutions (43) and (47) to map (49), we have

$$\begin{aligned}
\Delta x'_{20} &= \tilde{f}_1^{\mathrm{II}}(\Delta x_{20}, \Delta \dot{x}_{20}, \Delta\tau, \Delta t_s, \Delta t_f) \overset{Def}{=} f_1^{\mathrm{II}}(\Delta x_{20}, \Delta \dot{x}_{20}, \Delta\tau),\\
\Delta \dot{x}'_{20} &= \tilde{f}_2^{\mathrm{II}}(\Delta x_{20}, \Delta \dot{x}_{20}, \Delta\tau, \Delta t_s, \Delta t_f) \overset{Def}{=} f_2^{\mathrm{II}}(\Delta x_{20}, \Delta \dot{x}_{20}, \Delta\tau),\\
\Delta\tau' &= \Delta\tau + \omega\Delta t_s + \omega\Delta t_f \overset{Def}{=} f_3^{\mathrm{II}}(\Delta x_{20}, \Delta \dot{x}_{20}, \Delta\tau).
\end{aligned} \tag{51}$$

Let $V$ denote some neighbourhood of the origin in $\mathbf{R}^3$, map (49) $f_v^{\mathrm{II}}: V \to \mathbf{R}^3$ may be expressed briefly as

$$\Delta X' = f^{\mathrm{II}}(v, \Delta X), \tag{52}$$

in which $v$ is a real parameter, $v \in \mathbf{R}^1$, $\Delta X = (\Delta x_{20}, \Delta \dot{x}_{20}, \Delta\tau)^{\mathrm{T}}$, $\Delta X' = (\Delta x'_{20}, \Delta \dot{x}'_{20}, \Delta\tau')^{\mathrm{T}}$, $f^{\mathrm{II}}(v, \Delta X) = (f_1^{\mathrm{II}}, f_2^{\mathrm{II}}, f_3^{\mathrm{II}})^{\mathrm{T}}$.

Linearizing map (51) at the $n-1-$(II) fixed point results in the matrix

$$Df^{\mathrm{II}}(v, 0) = \begin{pmatrix} \dfrac{\partial f_1^{\mathrm{II}}}{\partial \Delta x_{20}} & \dfrac{\partial f_1^{\mathrm{II}}}{\partial \Delta \dot{x}_{20}} & \dfrac{\partial f_1^{\mathrm{II}}}{\partial \Delta\tau} \\ \dfrac{\partial f_2^{\mathrm{II}}}{\partial \Delta x_{20}} & \dfrac{\partial f_2^{\mathrm{II}}}{\partial \Delta \dot{x}_{20}} & \dfrac{\partial f_2^{\mathrm{II}}}{\partial \Delta\tau} \\ \dfrac{\partial f_3^{\mathrm{II}}}{\partial \Delta x_{20}} & \dfrac{\partial f_3^{\mathrm{II}}}{\partial \Delta \dot{x}_{20}} & \dfrac{\partial f_3^{\mathrm{II}}}{\partial \Delta\tau} \end{pmatrix}_{(v,0,0,0)}, \tag{53}$$

where the elements of the matrix are given by

$$\frac{\partial f_i^{\mathrm{II}}}{\partial y_j} = \frac{\partial \tilde{f}_i^{\mathrm{II}}}{\partial y_j} + \frac{\partial \tilde{f}_i^{\mathrm{II}}}{\partial \Delta t_s}\frac{\partial \Delta t_s}{\partial y_j} + \frac{\partial \tilde{f}_i^{\mathrm{II}}}{\partial \Delta t_f}\frac{\partial \Delta t_f}{\partial y_j} \quad (i, j = 1, 2, 3). \tag{54}$$

If the system can exhibit periodic motion of $n-1-$(I) for some system parameter regions, the resultant force $F_1$, at the instant of impact, satisfies condition (6). Periodic solution of $n-1-$(I) orbit and its Poincaré map can be derived by using analytical method (see Appendix A). The Poincaré map, corresponding to $n-1-$(I) orbit, may be expressed briefly by

$$\Delta X' = f^{\mathrm{I}}(v, \Delta X), \tag{55}$$

where $v \in \mathbf{R}^1$, $\Delta X = (\Delta x_{20}, \Delta \dot{x}_{20}, \Delta\tau)^{\mathrm{T}}$, $\Delta X' = (\Delta x'_{20}, \Delta \dot{x}'_{20}, \Delta\tau')^{\mathrm{T}}$, $f^{\mathrm{I}}(v, \Delta X) = (f_1^{\mathrm{I}}, f_2^{\mathrm{I}}, f_3^{\mathrm{I}})^{\mathrm{T}}$.

There existing two types of period $n$ single-impact motions in the plastic vibro-impact system, the map of period $n$ single-impact orbit consists of two piecewise parts, and that both are all three-dimensional and have the same variables. The $n$–1–(I) periodic motion may be taken as a special case of $n-1-$(II) periodic motion, i.e., the case of $t_s = 0$. For convenience of notation, we use $f(v, \Delta X)$ to denote the Poincaré map of period $n$ single-impact orbit in plastic vibro-impact case, i.e.,

$$f(v, \Delta X) = \begin{cases} f^{\mathrm{II}}(v, \Delta X), & v \text{ corresponding to } n-1-\text{(II) orbit},\\ f^{\mathrm{I}}(v, \Delta X), & v \text{ corresponding to } n-1-\text{(I) orbit}. \end{cases} \tag{56}$$

## 4. LOCAL STABILITY FOR $n-1$ ORBIT

The local stability of period $n$ single-impact orbits is determined by computing eigenvalues of $Df(v, 0)$. If all eigenvalues of $Df(v, 0)$ are inside the unit circle, then the

corresponding periodic orbit and fixed points are stable; otherwise, they are unstable. If the eigenvalues of $Df(v, 0)$ with the largest modules lie on the unit circle when $v = v_c$ ($v_c$ is a bifurcation value), then there is the possibility of bifurcations taking place. In general, bifurcations occur in various ways according to the number of eigenvalues on the unit circle and their position on the unit circle, resulting in qualitative changes of the system dynamics. If $Df(v, 0)$ has a pair of simple complex non-real eigenvalues, crossing the unit circle as $v$ passes $v_c$; the remainder of the spectrum of $Df(v,0)$ will be assumed to stay strictly inside the unit circle, it is possible that Hopf bifurcation of period $n$ single-impact orbit may take place. If $Df(v,0)$ has a real eigenvalue, crossing the unit circle from point $(-1, 0)$ as $v$ passes $v_c$; the remainder of the spectrum of $Df(v,0)$ are strictly inside the unit circle, period-doubling bifurcation of period $n$ single-impact orbit can occur.

There exist two types of period $n$ single-impact motions in the system, so the Poincaré map of period $n$ single-impact orbits is more complicated than that of the elastic impact system [18, 20]. Equations of $n-1-$(II) fixed point and sticking time $t_s$ may be determined by combining boundary conditions (27) to expressions (24) of $n-1-$(II) periodic motion, but the equations are transcendental ones. For this reason, the expressions of $n-1-$(II) periodic motion and Poincaré map of the system shown in Figure 1 cannot be obtained in closed form like those of single-degree-of-freedom systems in inelastic vibro-impact case [9–11]. The $n-1-$(I) periodic motion and Poincaré map can be determined analytically. In the linearizing matrix $Df^{\mathrm{II}}(v,0)$ of the map $f^{\mathrm{II}}(v, \Delta X)$, only $n-1-$(II) fixed point $X^* = (x_{20}, x_{20}, \tau_0)^{\mathrm{T}}$ and sticking time $t_s$ are unknown, but stable fixed point $X^* = (x_{20}, x_{20}, \tau_0)^{\mathrm{T}}$ and $t_s$ may be obtained by numerical simulation. Eigenvalues of $Df^{\mathrm{II}}(v,0)$, corresponding stable $n-1-$(II) orbit, may be computed by inserting $X^* = (x_{20}, x_{20}, \tau_0)^{\mathrm{T}}$ and $t_s$ obtained by numerical computation, into matrix (55). The bifurcating value of period $n$ single-impact orbit may be determined approximately via this way. When control parameter $v$ varies to some critical value $v_c$, the period $n$ single-impact orbit will change its stability, and eigenvalues of $Df(v,0)$ with largest models are on the unit circle at the corresponding critical value $v_c$.

The vibro-impact system with system parameters $\mu_m = 1$, $\mu_k = 1$, $\zeta = 0{\cdot}1$, $b = 0$, $\bar{f}_{20} = 0$, $v = \omega$ has been chosen to be analyzed. It is shown by numerical results that the system shown in Figure 1 can exhibit stable period 1 single-impact orbit for $\omega \in [1{\cdot}3, 1{\cdot}817465]$. As $\omega = 1{\cdot}81749$, the period 1 single-impact orbit of the system has changed its stability and stable period 2 two-impact orbit are created. Local bifurcation diagram of $n-1$ orbit is plotted in the ($\omega t_f/2\pi$, $\omega(t_f + t_s)/2\pi$ and $\dot{x}_{1-}$ versus $\omega$) planes as shown in Figure 3, from which we can observe transition from $n-1-$(II) motion to $n-1-$(I) one with increase in control parameter $\omega$. In Figure 3, there are three windows of periodic motions with single impact for $\omega = 0{\cdot}5 - 4{\cdot}5$, i.e., $n = 1, 2, 3$. In Figure 3(a), the parts of oblique lines

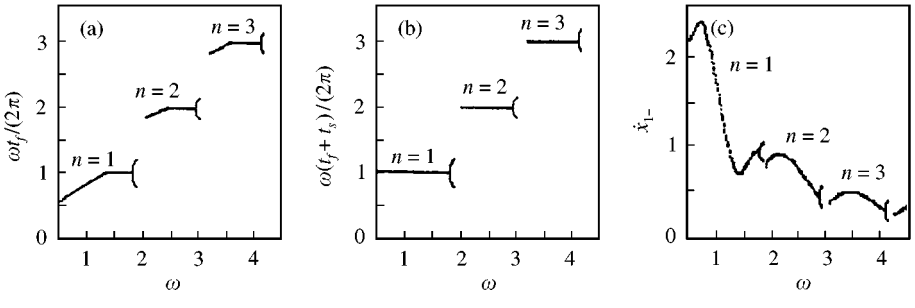


Figure 3. Local bifurcation diagram of $n-1$ orbits for the system with $\mu_m = 1$, $\mu_k = 1$, $\zeta = 0{\cdot}1$, $b = 0$, $\bar{f}_{20} = 0$, $v = \omega$, ($n = 1, 2, 3$).

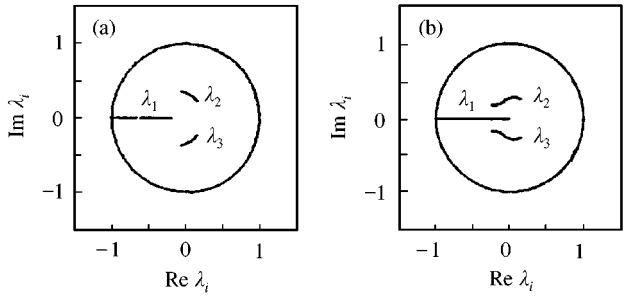


Figure 4. Variation of eigenvalues inside the unit circle: (a) $n = 1$, $\omega \in [1{\cdot}3,\ 1{\cdot}817465]$; (b) $n = 2$, $\omega \in [2{\cdot}05,\ 2{\cdot}913915]$.

correspond to $n - 1 -$ (II) orbits, the parts of level lines to $n - 1 -$ (I) orbits. It is certain that period $n$ single-impact orbit develops in a regular manner as $\omega$ is increased. In the parameter region of stable $n - 1$ orbit, there exists stable $n - 1 -$ (II) orbit in low $\omega$ region, then transition from $n - 1 -$ (II) orbit to $n - 1 -$ (I) one occurs with increase in $\omega$. Taking $n = 1$ and inserting 1–1 fixed points $X^* = (x_{20}, \dot{x}_{20}, \tau_0)^{\mathrm{T}}$ and sticking time $t_s$ obtained by numerical computation for $\omega \in [1{\cdot}3,\ 1{\cdot}817465]$, into matrix (53), we can compute the eigenvalues of $Df(\omega, 0)$ on the same parameter interval. It is shown that all eigenvalues of $Df(\omega,0)$ stay strictly inside the unit circle for $\omega \in [1{\cdot}3,\ 1{\cdot}817465]$, with $\lambda_1$ being real, $\lambda_2$ and $\lambda_3$ being a pair of complex conjugate eigenvalues. As $\omega = 1{\cdot}817465$, $\lambda_1 = -0{\cdot}99999961$ and $|\lambda_{2,3}| < 1$, $\lambda_1$ is extremely close to $-1$, the parameter value $\omega = 1{\cdot}817465$ may be approximately assumed to be a period-doubling bifurcation value of 1–1 orbit. The variation of the eigenvalues of $Df(\omega,0)$ is shown for $\omega \in [1{\cdot}3,\ 1{\cdot}817465]$ in Figure 4(a), in which $|\lambda_1|$ increases with increase in $\omega$.

The system has stable period 2 single-impact orbits for $\omega \in [2{\cdot}05,\ 2{\cdot}913915]$. When $\omega = 2{\cdot}91393$, the period 2 single-impact orbit has changed its stability and stable period 4 two-impact orbit is created. Taking $n = 2$ and inserting $2 - 1$ fixed points $X^* = (x_{20}, x_{20}, \tau_0)^{\mathrm{T}}$ and $t_s$ obtained by numerical computation, into matrix (53), we find that all eigenvalues of $Df(\omega,0)$ stay strictly inside the unit circle for $\omega \in [2{\cdot}05,\ 2{\cdot}913915]$, with real eigenvalue $\lambda_1$ and a pair of complex conjugate eigenvalues $\lambda_2$ and $\lambda_3$. As $\omega = 2{\cdot}913915$, $\lambda_1 = -0{\cdot}99999936$, and $|\lambda_{2,3}| < 1$, $\lambda_1$ is extremely close to $-1$, so the parameter value $\omega = 2{\cdot}913915$ may be approximately assumed to be a period-doubling bifurcation value of period 2 single-impact orbit. The variation of the eigenvalues of $Df(\omega,0)$ is shown for $\omega \in [2{\cdot}05,\ 2{\cdot}913915]$ in Figure 4(b). Here we compute only eigenvalues of $Df(\omega,0)$ corresponding stable $n - 1$ orbits by the way, thus stable $n - 1$ orbits, obtained by numerical simulation, are verified by the analyses of eigenvalues, and approximate bifurcation values of period-doubling are determined.

## 5. GLOBAL BIFURCATIONS

To bring out the essential dynamical features of the system, the bifurcational behaviours are studied to unfold the dynamic evolution of the system beyond period-doubling bifurcations. The system, with system parameters $\mu_m = 1$, $\mu_k = 1$, $\zeta = 0{\cdot}1$, $b = 0$, $\bar{f}_{20} = 0$, has been chosen for analysis, and the excitation frequency $\omega$ is taken as a control parameter. Some results are presented in the form of bifurcation diagrams, periodic response and phase plane diagrams. In Figures 5–11 periodic response ($\dot{x}_1 - \omega t$) and their phase plane portraits ($\dot{x}_1 - x_1$) are plotted. As $\omega \in [2{\cdot}05,\ 2{\cdot}49015)$, the system can exhibit stable period

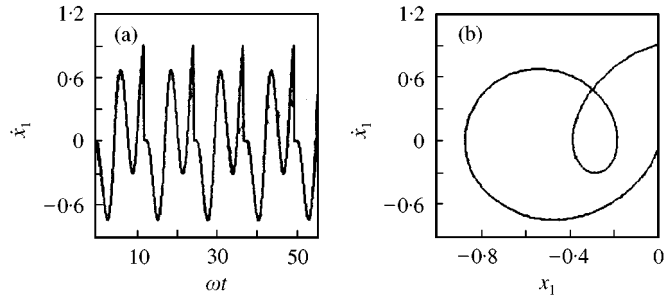


Figure 5. $2-1-$(II) periodic motion ($\omega = 2{\cdot}1$).

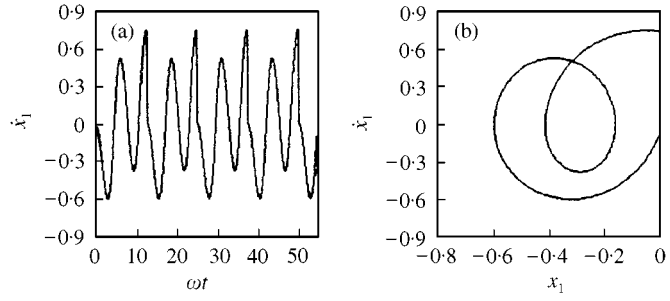


Figure 6. $2-1-$(I) periodic motion ($\omega = 2{\cdot}5$).

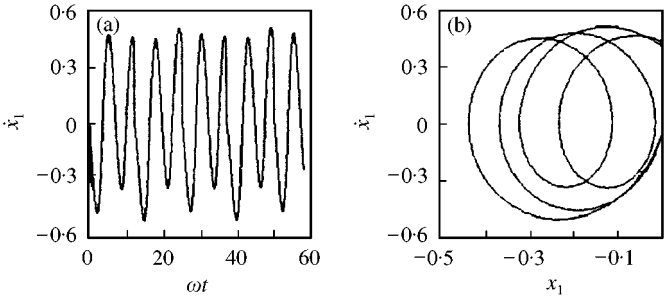


Figure 7. $4-2-$(I) periodic motion ($\omega = 2{\cdot}921$).

2 single-impact orbit, corresponding $2-1-$(II) motion. This implies that $2-1$ orbit in the interval is degenerate in the sense that the mass $M_1$ simply follows the stop until the resultant force $F_1$ acted on the mass $M_1$ change its sign and begins to push the mass $M_1$ away from the stop. As $\omega$ is increased further, the $2-1-$(II) orbit vanishes and $2-1-$(I) orbit is generated. For $\omega \in [2{\cdot}49015,\ 2{\cdot}913915)$, the system has stable $2-1-$(I) orbit. A stable $2-1-$(II) response of the mass $M_1$ is shown for $\omega = 2{\cdot}1$ in Figure 5. Response and phase plane portraits of stable of $2-1-$(I) orbit are plotted for $\omega = 2{\cdot}5$ in Figure 6.

As we have known, for the $2-1-$(I) orbit at $\omega = \omega_c = 2{\cdot}913915$, $Df(\omega,0)$ has a real eigenvalue $\lambda_1$ extremely close to the point $(-1, 0)$. When $\omega$ passes $\omega_c$, $2-1-$(I) orbit has changed its stability, and stable $4-2-$(I) periodic orbit bifurcates from $2-1-$(I) one. Response and phase plane portraits of the mass $M_1$ are shown for $\omega = 2{\cdot}921$ in Figure 7,

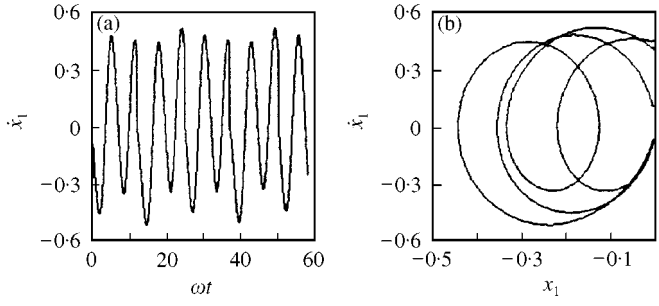


Figure 8. $4-2-$(II) periodic motion with grazing boundary ($\omega = 2{\cdot}924938$).

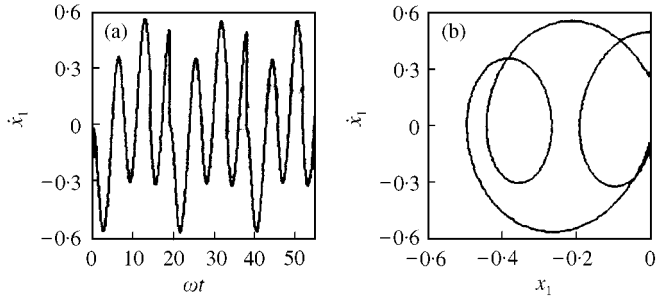


Figure 9. $3-2-$(II) periodic motion ($\omega = 3{\cdot}02$).

from which we find that the system can exhibit stable $4-2-$(I) orbit at $\omega = 2{\cdot}921$. As $\omega = 2{\cdot}922423$, the system begins to exhibit $4-2-$(II) orbit, which means that the mass $M_1$ is stuck to the stop for duration $t_s$ after some impact and the original system becomes a single-degree-of-freedom oscillator with the mass $M_2$. As $\omega$ is increased to $\omega = 2{\cdot}924938$, the system exhibits the $4-2-$(II) orbit with "grazing boundary", i.e., the mass $M_1$ impacts the stop with zero velocity (i.e., $\dot{x}_{1-} = 0$), which results in singularity of Poincaré map and qualitative changes of the system dynamics. Such a case of $4-2-$(II) orbit with grazing boundary is shown for $\omega = 2{\cdot}924938$ in Figure 8. Because of $4-2-$(II) orbit with grazing boundary, there does not exist $8-4-$(II) motion bifurcating from $4-2-$(II) orbit, as we will see in Figures 12 and 14, period-doubling cascades of $2-1$ orbit do not occur. With the $4-2-$(II) orbit with grazing boundary occurring, the $4-2-$(II) periodic orbit undergoes a sequence of transitions that change it to $3-2-$(II) orbit with increase in $\omega$. An orbit of $3-2-$(II) is given for $\omega = 3{\cdot}02$ in Figure 9. As $\omega$ is increased to $\omega = 3{\cdot}03419$, grazing boundary phenomenon occurs again so as to result in a transition that changes $3-2-$(II) orbit to $3-1-$(II) one. Such a case of transition is shown in Figures 9–11, and the phase plane portrait of the $3-1-$(II) orbit with grazing boundary is shown in Figure 10. With further increase in control parameter $\omega$, $3-1-$(II) orbit disappears, sticking time $t_s$ of the mass $M_1$ has shrunk to zero and $3-1-$(I) orbit is created. A bifurcation diagram of period 2 single-impact orbit is plotted in the ($\omega t_f/(2\pi)$ and $\dot{x}_{1-}$ versus $\omega$) planes as shown in Figure 12. As we can see in Figure 12, the period-doubling bifurcation of period 2 single-impact orbit is existent, but the period-doubling cascades is non-existent under a smooth change in the excitation frequency. After period-double bifurcation of period 2 single-impact orbit occurs, the system exhibits the motions with grazing boundary, which result in the period-doubling cascades of period 2 single-impact orbits non-existent, so that

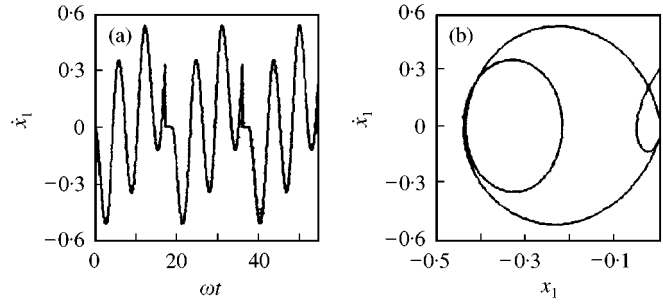


Figure 10. $3-1-$(II) periodic motion with grazing boundary ($\omega = 3{\cdot}03419$).

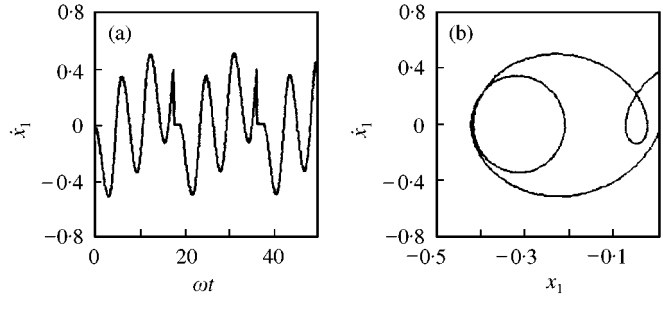


Figure 11. $3-1-$(II) periodic motion ($\omega = 3{\cdot}1$).

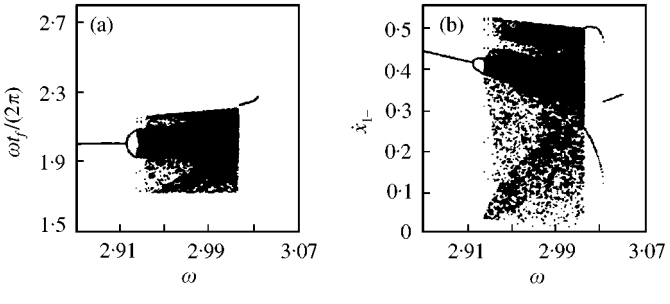


Figure 12. Doubling-period bifurcation diagram for the system with $\mu_m = 1$, $\mu_k = 1$, $\zeta = 0{\cdot}1$, $b = 0$, $\bar{f}_{20} = 0$, $\omega = 2{\cdot}87 \sim 3{\cdot}065$.

extremely long periodic and chaotic motions are generated immediately. Such a route to chaos via grazing boundary is apparent in Figure 12. A bifurcation diagram for period $n$ single-impact orbit is plotted for $\omega = 0.5$–10 in the ($\omega t_f/2\pi$ and $\dot{x}_{1-}$ versus $\omega$) planes as shown in Figure 13. For other $n-1$ orbits ($n = 1, 3, 4, \ldots, 7$), as we have computed and analyzed in Figure 13, transitions of two types of periodic motions and dynamic evolution beyond period-doubling bifurcations are similar to those of $2-1$ orbit. By analyses of numerical results for $\omega = 0.5$–10, the global bifurcation process of $n-1$ orbit ($n = 1, 2, 3, \ldots, 7$) may be summarized:

$n-1-$(II) $\rightarrow n-1-$(I) $\rightarrow 2n-2-$(I) $\rightarrow 2n-2-$(II) $\rightarrow 2n-2-$(II) orbit with "grazing boundary" $\rightarrow$ extremely long periodic orbits and chaos $\rightarrow (n+1)-2-$(II) $\rightarrow (n+1)-1-$(II) orbit with "grazing boundary" $\rightarrow (n+1)-1-$(II) $\rightarrow (n+1)-1-$(I).

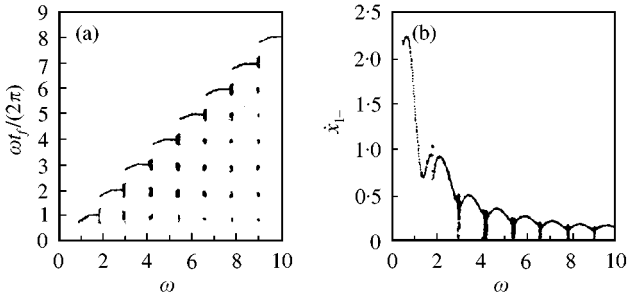


Figure 13. Global bifurcation diagram for the system with $\mu_m = 1$, $\mu_k = 1$, $\zeta = 0{\cdot}1$, $b = 0, f_{20} = 0$.

Period-doubling cascades of $n-1$ orbit do not occur, and grazing boundary phenomena cause $2n-2-(\mathrm{II})$ orbit to undergo a sequence of transitions that change it to $(n+1)-1-(\mathrm{II})$ orbit. These transitions are not regular bifurcations but arise from piecewise property of the map and singularity caused by the motion with grazing boundary.

## 6. THE INFLUENCE OF SYSTEM PARAMETERS ON PERIODIC IMPACTS AND BIFURCATIONS

The two-degree-of-freedom system studied here involves six system parameters: $\omega$, $\mu_m$, $\mu_k$, $\zeta$, $b$, $\bar{f}_{20}$. Due to this relatively large number of parameters, the detailed influence of all parameters on the system dynamics is not presented here. However, it is of interest to analyze the influence of some system parameter on the system dynamics. Taking system parameters $\mu_m = 2$, $\mu_k = 5$, $\zeta = 0{\cdot}1$, $b = 0, f_2 = 0$ as criterion, we analyze the influence of system parameters such as distribution of mass and stiffness, damping ratio on harmonic and subharmonic resonances. Thus, some bifurcation diagrams are presented. Global bifurcation diagram is shown for $\omega = 0{\cdot}5$–$10$ in Figure 14(a). In most cases we observe the typical behaviour, with periodic windows with one impact velocity, separated by other periodic or chaotic regions. From these figures we can observe that the period of the motion with one impact in the periodic window number $j$ is $j$ times the period of the forcing. Increased damping generally results in lower impact velocities and larger regions of periodic windows with single-impact orbit as seen in Figure 14(b). Low damping, Figure 14(c), leads to larger impact velocities. For low $\mu_m$ and large $\mu_k$, the system exhibits similar behaviour, and there exist larger regions of $n-1$ orbits; see Figure 14(d) and 14(e). The number of periodic windows with single-impact orbit increases remarkably for low $\mu_k$, but regions of $n-1$ orbits shrink and areas of long periodic and chaotic motions enlarge, see Figure 14(f). Large $\mu_m$, Figure 14(g), results in lower impact velocity, and regions of $n-1$ orbits shrink and areas of long-periodic and chaotic motions enlarge slightly. Parameters $\bar{f}_{10}$ and $\bar{f}_{20}$ satisfy the relationship: $\bar{f}_{10} + \bar{f}_{20} = 1$. As $\bar{f}_{20}$ increases, impact velocity of the mass $M_1$ decreases, and regions of chaotic motions enlarge; see Figure 14(h). As the parameter $b > 0$, the number of periodic windows with single-impact orbit decreases. For example, there exist only period 1 single-impact and period 2 single-impact orbits for $b = 0.2$; see Figure 14(i). (Only changed parameter is given in Figure 14(b)–(i), and all the other parameters, not given, are the same as criterion parameters.)

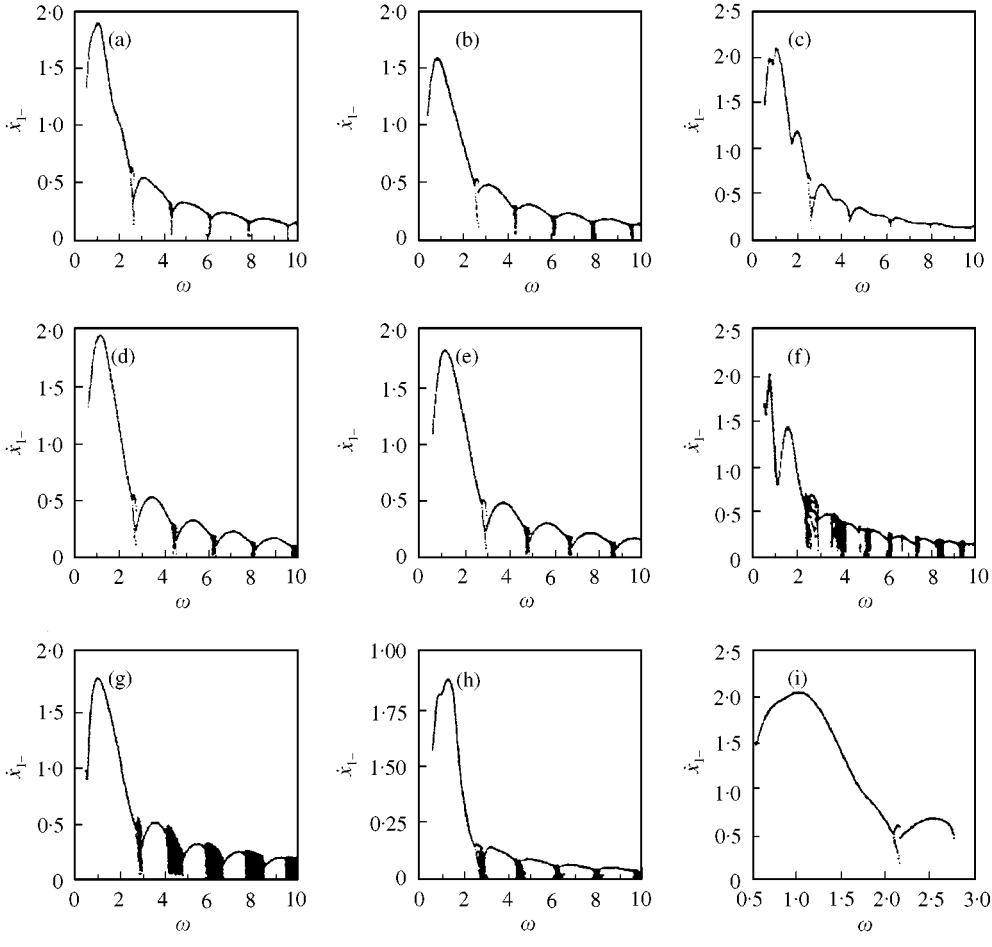


Figure 14. Global bifurcation diagrams of the plastic vibro-impact system: (a) $\mu_m = 2$, $\mu_k = 5$, $\zeta = 0{\cdot}1$, $b = 0$, $\bar{f}_{20} = 0$; (b) $\zeta = 0{\cdot}2$; (c) $\zeta = 0{\cdot}05$; (d) $\mu_m = 0{\cdot}7$; (e) $\mu_k = 16$; (f) $\mu_k = 1{\cdot}5$; (g) $\mu_m = 20$; (h) $f_1 = 0{\cdot}3$, $\bar{f}_{20} = 0{\cdot}7$; (i) $b = 0{\cdot}2$.

## 7. CONCLUSION

The motions of single-degree-of-freedom plastic vibro-impact oscillators were studied by using one-dimensional maps, which are piecewise on circle [9–11]. Dynamics and bifurcations of the oscillator considered in references [9, 10], in elastic vibro-impact case, was investigated in reference [21]. It is found that periodic motions and their bifurcations of the oscillator, in plastic impact case [9, 10], are distinct from those in elastic impact case [21]. In general, the period-doubling cascades of single-impact orbits are existent, but discontinued in elastic vibro-impact systems. On the perfectly plastic impact condition, dynamics of the two-degree-of-freedom system with harmonic excitations and a constraint may be represented by a three-dimensional map. The map consists of two parts, and one of them, corresponding to $n - 1 -$ (I) orbit, cannot be obtained in closed form like those of single-degree-of-freedom plastic vibro-impact oscillators [9–11]; the other, corresponding to $n - 1 -$ (I) orbit, can be derived by using analytical method used in references [18, 20]. Stable $n - 1 -$ (II) orbits may be verified by the local stability analysis discussed in the previous section. There exist singularities in the system like in the elastic vibro-impact systems, which are caused by the motion with grazing boundary. Moreover, the map of the

plastic vibro-impact system is piecewise. The influence of the piecewise property and singularities on global bifurcations and transition to chaos is elucidated. It is found that the vibro-impact system goes through complicated dynamic evolution beyond period-doubling bifurcations with increase in the excitation frequency. Period-doubling bifurcations of $n-1$ orbit taking place in the plastic vibro-impact system are qualitatively very much different from those in elastic vibro-impact systems [20, 21]. Period-doubling bifurcations of single-impact orbits are commonly existent in the plastic vibro-impact system, but the period-doubling cascades do not occur under a smooth change in the excitation frequency. The motions with grazing boundary result in that the period-doubling cascades of single-impact orbits do not occur so that extremely long periodic and chaotic motions are generated immediately. This means that a sequence of transitions occur via the motion with grazing boundary so that they change a period $2n$ two-impact orbit to a period $n+1$ single-impact orbit. These transitions are not regular bifurcations but arise from two respects of reasons, i.e., the piecewise property of the map and its singularity caused by the motions with grazing boundary. The method of dynamical analysis of the model in Figure 1 can be applied to some vibratory impact machines and equipment, for example pile driver, compacting and forming machinery, etc. Global dynamical analyses for plastic vibro-impact systems have important significance on optimization design of machinery with plastic vibro-impact.

## ACKNOWLEDGMENT

The authors gratefully acknowledge the support by the National Science Foundation of China (10072051) and the Provincial Science Foundation of Gansu (ZR-97-039), China.

## REFERENCES

1. A. B. NORDMARK 1991 *Journal of Sound and Vibration* **145**, 279–297. Non-periodic motion caused by grazing incidence in an impact oscillator.
2. G. S. WHISTON 1992 *Journal of Sound and Vibration* **152**, 427–460. Singularities in vibro-impact dynamics.
3. F. PETERKA and J. VCACIK 1992 *Journal of Sound and Vibration* **154**, 95–115. Transition to chaotic motion in mechanical systems with impacts.
4. S. FOALE and S. R. B. IISHOP 1994 in *Nonlinearity and Chaos in Engineering Dynamics* (J. M. T. Thompson, editor). 91–102. Chichester: John Wiley & Sons Ltd. Bifurcations in impact oscillators: theory and experiments.
5. A. P. IVANOY 1993 *Journal of Sound and Vibration* **162**, 562–565. Stabilization of an impact oscillator near grazing incidence owing to resonance.
6. A. P. IVANOY 1996 *Chaos, Solitons and Fractals* **7**, 1615–1634. Bifurcation in impact systems.
7. F. PETERKA 1996 *Chaos, Solitons and Fractals* **7**, 1635–1647. Bifurcation and transition phenomena in an impact oscillator.
8. K. M. CONE and R. I. ZADOKS 1995 *Journal of Sound and Vibration* **188**, 660–683. The effect of frequency and clearance variations on single-degree-of-freedom impact oscillators.
9. S. W. SHAW and P. J. HOLMES 1983 *Journal of Applied Mechanics* **50**, 894–857. A periodically forced impact oscillator with large dissipation.
10. S. W. SHAW and P. J. HOLMES 1983 *Physical Review Letters* **51**, 894–857. Periodically forced linear oscillator with impacts: chaos and long-period motions.
11. J.-H. XIE 1997 *Acta Mechanics Sinica* **29**, 456–463. The mathematical model for the impact hammer and global bifurcations.
12. F. PETERKA 1993 *Journal of Sound and Vibration* **165**, 369–372. Letters to the editor: Comments on "Periodic and chaotic behaviour of a threshold-limited two-degree-of-freedom system".

13. J.-H. XIE 1996 *Applied Mathematics and Mechanics* **17**, 65–75. Codimension two bifurcations and Hopf bifurcations of an impacting vibrating system.
14. C. BUDD, F. DUX and A. CLIFFE 1995 *Journal of Sound and Vibration* **184**, 475–502. The effect of frequency and clearance variations on single-degree-of-freedom impact oscillators.
15. S. NATSIAVAS 1993 *Journal of Sound and Vibration* **165**, 439–453. Dynamics of multiple-degree-of-freedom oscillators with colliding components.
16. S. NATSIAVAS and H. GONZALEZ 1992 *Journal of Applied Mechanics* **59**, 284–290. Vibration of harmonically excited oscillators with asymmetric constraints.
17. S. CHATTERJEE and A. K. MALIK 1996 *Journal of Sound and Vibration* **191**, 539–562. Bifurcations and chaos in autonomous self-excited oscillators with impact damping.
18. G. W. LUO and J.-H. XIE 1998 *Journal of Sound and Vibration* **213**, 391–408. Hopf bifurcation of a two-degree-of-freedom vibro-impact system.
19. J. GUCKENHEIMER, P. HOLMES, 1983 *Nonlinear Oscillations, Dynamical Systems, and Bifurcations of Vector Fields*. Springer-Verlag, New York Berlin Heidelberg Tokyo.
20. J. O. AIDANPÄÄ and R. B. GUPTA 1993 *Journal of Sound and Vibration* **165**, 305–327. Periodic and chaotic behaviour of a threshold-limited two-degree-of-freedom system.
21. S. W. SHAW and P. J. HOLMES 1983 *Journal of Sound & Vibration* **90**, 129–155. A periodically forced piecewise linear oscillator.

## APPENDIX A

The determination of $n-1-(\mathrm{I})$ periodic solutions is based on the fact that they satisfy the following set of periodicity and matching conditions

$$x_1(0)=b, \qquad x_1(2n\pi/\omega)=b, \qquad \dot{x}_1(0)=0, \qquad x_2(0)=x_2(2n\pi/\omega), \qquad \dot{x}_2(0)=\dot{x}_2(2n\pi/\omega). \tag{A1}$$

For convenience of expression, we give expression for some symbols $h$, $l_j$ and $\bar{l}_j$ firstly:

$$h=\left(\frac{\psi_{22}\bar{l}_2\omega}{\psi_{11}\psi_{12}l_1\bar{l}_2-\psi_{12}\psi_{21}\bar{l}_1l_2}\right)\left(\frac{\psi_{11}e_1s_1}{1-e_1c_1}-\frac{\psi_{12}e_2s_2}{1-e_2c_2}\frac{\psi_{21}\bar{l}_1}{\psi_{22}\bar{l}_2}\right), \tag{A2}$$

$$l_j=\frac{e_j\eta_js_j}{1-e_jc_j}-\omega_{dj}, \qquad \bar{l}_j=\frac{\omega_{dj}e_j(c_j-e_j)}{1-e_jc_j}-\omega_{dj} \quad (j=1,2), \tag{A3}$$

where $s_j=\sin(2n\pi\omega_j/\omega)$, $c_j=\cos(2n\pi\omega_j/\omega)$, $e_j=\mathrm{e}^{-\eta_j 2n\pi/\omega}$, $j=1,2$.

The $n-1-(\mathrm{I})$ periodic solutions are given by

$$x_i(t)=\sum_{j=1}^{2}\psi_{ij}\xi_j(t), \qquad \dot{x}_t(t)=\sum_{j=1}^{2}\psi_{ij}\dot{\xi}_j(t) \quad (t=0 \bmod 2n\pi/\omega), \tag{A4}$$

where $\xi_j(t)=\mathrm{e}^{-\eta_j t}(a_j\cos\omega_{dj}t+b_j\sin\omega_{dj}t)+A_j\sin(\omega t+\tau_0)+B_j\cos(\omega t+\tau_0)$.

If $b=0$, then let $\tau_0=\bar{\tau}_0$,

$$\bar{\tau}_0=\tan^{-1}\left(\frac{hd_1+d_2}{hd_2-d_1}\right), \tag{A5}$$

otherwise

$$\tau_0=\cos^{-1}\left(\frac{\bar{x}_{10}\tan\bar{\tau}_0\pm\sqrt{\tan^2\bar{\tau}_0-\bar{x}_{10}^2+1}}{\tan^2\bar{\tau}_0+1}\right), \tag{A6}$$

where

$$d_1 = \sum_{j=1}^{2} \psi_{1j} A_j, \qquad d_2 = \sum_{j=1}^{2} \psi_{1j} B_j, \qquad \bar{x}_{10} = \frac{b}{(hd_2 - d_1)},$$

$$a_j = \frac{e_j b_j s_j}{1 - e_j c_j} \quad (j = 1, 2), \tag{A7}$$

$$b_1 = \frac{\psi_{22}\bar{l}_2\omega(d_1 \cos\tau_0 - d_2 \sin\tau_0)}{\psi_{11}\psi_{12}l_1\bar{l}_2 - \psi_{12}\psi_{21}\bar{l}_1 l_2}, \qquad b = -\frac{\psi_{21}\bar{l}_1\omega(d_1 \cos\tau_0 - d_2 \sin\tau_0)}{\psi_{11}\psi_{12}l_1\bar{l}_2 - \psi_{12}\psi_{21}\bar{l}_1 l_2}. \tag{A8}$$

The other symbols $\omega_{dj}$, $\eta_j$, $\psi_{ij}$, $A_j$ and $B_j$ are the same as those in the second chapter.

The existence of periodic impacts requires the condition

$$\tan^2\bar{\tau}_0 - \bar{x}_{10}^2 + 1 \geqslant 0, \qquad \left| \frac{\bar{x}_{10}\tan\bar{\tau}_0 \pm \sqrt{\tan^2\bar{\tau}_0 - \bar{x}_{10}^2 + 1}}{\tan^2\bar{\tau}_0 + 1} \right| \leqslant 1. \tag{A9}$$

We can obtain the fixed point $X^* = (\dot{x}_{20}, x_{20}, \tau_0)^{\mathrm{T}}$ of $n-1-(\mathrm{I})$ orbit by inserting $t = 0$ into the periodic solutions (A4), i.e., $x_{20} = x_2(0)$, $\dot{x}_{20} = \dot{x}_2(0)$, $\tau = \tau_0$.

We consider the perturbed motion of $n-1-(\mathrm{I})$ orbit to determine the equation of map. For simplicity of notation, the origin of time is chosen at the impact point. The origin of $\theta$-co-ordinate is displaced to an impact point $o_2$ in Figure 2. Between two consecutive impacts, the solutions of the perturbed motion are written in the form

$$\tilde{x}_i(t) = \sum_{j=1}^{2} \psi_{ij}\tilde{\xi}_j(t), \qquad \dot{\tilde{x}}_i(t) = \sum_{j=1}^{2} \psi_{ij}\dot{\tilde{\xi}}_j(t) \quad (i = 1, 2), \tag{A10}$$

where

$$\begin{aligned}
\tilde{\xi}_j(t) &= \mathrm{e}^{-\eta_j t}(\tilde{a}_j \cos\omega_{dj}t + \tilde{b}_j \sin\omega_{dj}t) + A_j \sin(\omega t + \tau_0 + \Delta\tau) + B_j \cos(\omega t + \tau_0 + \Delta\tau),\\
\dot{\tilde{\xi}}_j(t) &= \mathrm{e}^{-\eta_j t}(\tilde{b}_j\omega_{dj} - \tilde{a}_j\eta_j)\cos\omega_{dj}t - (\tilde{b}_j\eta_j + \tilde{a}_j\omega_{dj})\sin\omega_{dj}t + A_j\omega\cos(\omega t + \tau_0 + \Delta\tau)\\
&\quad - B_j\omega\sin(\omega t + \tau_0 + \Delta\tau).
\end{aligned} \tag{A11}$$

For the disturbed motion of $n-1-(\mathrm{I})$ orbit, the dimensionless time is set to zero directly after an impact, it becomes $(2n\pi + \Delta\theta)/\omega$ just before the next impact, and $\Delta\theta = \Delta\tau' - \Delta\tau$. Letting $t_e = (2n\pi + \Delta\theta)/\omega$, the boundary conditions at two successive impact points are expressed as

$$\begin{aligned}
&\tilde{x}_1(0) = b, \qquad \tilde{x}_1(t_e) = b, \qquad \dot{\tilde{x}}_1(0) = 0, \qquad \dot{\tilde{x}}_1(t_{e-}) = \dot{x}_{1-} + \Delta\dot{x}'_{1-}, \qquad \dot{\tilde{x}}_1(t_{e+}) = 0,\\
&\tilde{x}_2(0) = x_{20} + \Delta x_{20}, \qquad \tilde{x}_2(t_e) = x_{20} + \Delta x'_{20}, \qquad \dot{\tilde{x}}_2(0) = \dot{x}_{20} + \Delta\dot{x}_{20},\\
&\dot{\tilde{x}}_2(t_e) = \dot{x}_{20} + \Delta\dot{x}'_{20},
\end{aligned} \tag{A12}$$

where $\dot{\tilde{x}}_1(t_{e+}) = -R\dot{\tilde{x}}_1(t_{e-}) = 0$, $t_{e-}$ and $t_{e+}$ represent, respectively, the time shortly before and after the instant of the impact.

Substituting boundary conditions (A12) into equation (A10) for $t = 0$, we obtain

$$\tilde{a}_1 = \frac{1}{D}(\psi_{22}b - \psi_{12}x_{20} - \psi_{12}\Delta x_{20} - DA_1 \sin(\tau_0 + \Delta\tau) - DB_1 \cos(\tau_0 + \Delta\tau)), \tag{A13}$$

$$\tilde{a}_2 = \frac{1}{D}(-\psi_{21}b + \psi_{11}x_{20} + \psi_{11}\Delta x_{20} - DA_2 \sin(\tau_0 + \Delta\tau) - DB_2 \cos(\tau_0 + \Delta\tau)), \tag{A14}$$

$$\tilde{b}_1 = \frac{1}{D\omega_1}(\psi_{22}\eta_1 b - \psi_{12}(\dot{x}_{20} + \Delta\dot{x}_{20} + \eta_1 x_{20} + \eta_1 \Delta x_{20}) - D(A_1\omega + \eta_1 B_1)\cos(\tau_0 + \Delta\tau) + D(B_1\omega - \eta_1 A_1)\sin(\tau_0 + \Delta\tau)), \tag{A15}$$

$$\tilde{b}_2 = \frac{1}{D\omega_2}(-\psi_{21}\eta_2 b + \psi_{11}(\dot{x}_{20} + \Delta\dot{x}_{20} + \eta_2 x_{20} + \eta_2 \Delta x_{20}) - D(A_2\omega + \eta_2 B_2)\cos(\tau_0 + \Delta\tau) + D(B_2\omega - \eta_2 A_2)\sin(\tau_0 + \Delta\tau)), \tag{A16}$$

where $D = |\psi|$.

Substituting boundary conditions (A12) into equation (A10) for $t = t_e$, we obtain

$$\sum_{j=1}^{2} \psi_{1j}\tilde{\xi}_j(t_e) = b, \tag{A17}$$

$$\Delta x'_{20} = \sum_{j=1}^{2} \psi_{2j}\tilde{\xi}_j(t_e) - x_{20}, \quad \Delta\dot{x}'_{20} = \sum_{j=1}^{2} \psi_{2j}\dot{\tilde{\xi}}_j(t_e) - \dot{x}_{20}, \quad \Delta\tau' = \Delta\tau + \Delta\theta(\Delta x_{20}, \Delta\dot{x}_{20}, \Delta\tau). \tag{A18}$$

Defining a function $\tilde{g}(\Delta x_{20}, \Delta\dot{x}_{20}, \Delta\tau, \Delta\theta)$ as

$$\tilde{g}(\Delta x_{20}, \Delta\dot{x}_{20}, \Delta\tau, \Delta\theta) = \sum_{j=1}^{2} \psi_{1j}\tilde{\xi}_j(t_e) - b = 0. \tag{A19}$$

The conditions, under which there exist $n - 1 -$ (I) fixed points, give

$$\tilde{g}(\Delta x_{20}, \Delta\dot{x}_{20}, \Delta\tau, \Delta\theta)|_{(0,0,0,0)} = 0. \tag{A20}$$

Suppose $(\partial\tilde{g}/\partial\Delta\theta)_{(0,0,0,0)} \neq 0$, according to the implicit function theorem, equation (A20) can be solved as

$$\Delta\theta = \Delta\theta(\Delta x_{20}, \Delta\dot{x}_{20}, \Delta\tau), \quad \Delta\theta(0, 0, 0) = 0. \tag{A21}$$

Inserting equation (A21) into equation (A18), we get finally the Poincaré map, which are given by

$$\begin{aligned}
\Delta x'_{20} &= \tilde{f}_1^{\mathrm{I}}(\Delta x_{20}, \Delta\dot{x}_{20}, \Delta\tau, \Delta\theta) \overset{Def}{=} f_1^{\mathrm{I}}(\Delta x_{20}, \Delta\dot{x}_{20}, \Delta\tau),\\
\Delta\dot{x}'_{20} &= \tilde{f}_2^{\mathrm{I}}(\Delta x_{20}, \Delta\dot{x}_{20}, \Delta\tau, \Delta\theta) \overset{Def}{=} f_2^{\mathrm{I}}(\Delta x_{20}, \Delta\dot{x}_{20}, \Delta\tau),\\
\Delta\tau' &= \Delta + \Delta\theta(\Delta x_{20}, \Delta\dot{x}_{20}, \Delta\tau) \overset{Def}{=} f_3^{\mathrm{I}}(\Delta x_{20}, \Delta\dot{x}_{20}, \Delta\tau).
\end{aligned} \tag{A22}$$

Linearizing the Poincaré map at the fixed point results in the matrix

$$Df^{\mathrm{I}}(v,0)=\left.\begin{pmatrix}\dfrac{\partial f_1^{\mathrm{I}}}{\partial \Delta x_{20}} & \dfrac{\partial f_1^{\mathrm{I}}}{\partial \Delta \dot{x}_{20}} & \dfrac{\partial f_1^{\mathrm{I}}}{\partial \Delta \tau}\\ \dfrac{\partial f_2^{\mathrm{I}}}{\partial \Delta x_{20}} & \dfrac{\partial f_2^{\mathrm{I}}}{\partial \Delta \dot{x}_{20}} & \dfrac{\partial f_2^{\mathrm{I}}}{\partial \Delta \tau}\\ \dfrac{\partial f_3^{\mathrm{I}}}{\partial \Delta x_{20}} & \dfrac{\partial f_3^{\mathrm{I}}}{\partial \Delta \dot{x}_{20}} & \dfrac{\partial f_3^{\mathrm{I}}}{\partial \Delta \tau}\end{pmatrix}\right|_{(v,0,0,0)} . \tag{A23}$$

Let $\Delta X=(\Delta x_1, \Delta x_2, \Delta x_3)^{\mathrm{T}}$ denotes $\Delta X=(\Delta x_{20}, \Delta \dot{x}_{20}, \Delta \tau)^{\mathrm{T}}$. The elements in matrix (A23) are given by

$$\frac{\partial f_j^{\mathrm{I}}}{\partial \Delta x_i}=\frac{\partial \tilde{f}_j^{\mathrm{I}}}{\partial \Delta x_i}-\frac{\partial \tilde{f}_j^{\mathrm{I}}}{\partial \Delta \theta}\cdot\left(\frac{\partial \tilde{g}}{\partial \Delta x_i}\Big/\left(\frac{\partial \tilde{g}}{\partial \Delta \theta}\right)\right) \quad (i,j=1,2,3). \tag{A24}$$